Magnetically Actuated Micro Swimming of Bio-inspired Robots in Mini Channels

Fatma Zeynep Temel[1], Serhat Yesilyurt[2]

Mechatronics Program, Sabanci University, Istanbul, Turkey

[1]zeyneptemel@sabanciuniv.edu

[2]syesilyurt@sabanciuniv.edu

Abstract— **Untethered swimming microrobots have many advantages for biomedical applications such as targeted drug delivery, simple surgical tasks including opening of clogged arteries and as diagnostic tools. In this paper, swimming of microrobots is examined in water and glycerin filled channels. Propulsion of microrobots is enabled by means of an external magnetic field that rotates in the axial direction of the channel and forces robots to rotate about the axis of the helical tail. Rotation of the helical tail resulted in a screw-like motion of the robot reaching speeds up to several millimeters per second for a 2-mm long robot. The results are compared with resistive force theory, which is based on the assumption that the propulsive force resulting from the rotation of the helix is proportional to the local velocity on the helical flagellum in low Reynolds number micro and viscous flows.**

Keywords— **Untethered micro swimmer, magnetic actuation, helical wave propagation, medical robotics, resistive force theory**

I. INTRODUCTION

Manufacturing of integrated devices with electrical, mechanical, chemical and biological components at very small scales enables numerous opportunities to improve on broad range of applications of technology, science and medicine. Controlled motion of microscale [1, 2] and nanoscale [3] robots in fluidic environments are demonstrated. It is well established that these microrobots can be used in many biological and medical applications including minimally invasive surgical procedures and systems [4, 5].

Design and characterization of microrobots for minimally invasive surgery (MIS) have become increasingly popular in recent years. Sudo et al. used microrobots on the order of millimeter, propagating with planar waves and studied the effect of tail width and length on the swimming velocity [6]. Dreyfus et al. used planar wave propagation by linking superparamagnetic colloids with double stranded DNAs which has a total length of 24 μm and showed that the velocity and direction of motion is controlled by adjusting the external fields [1]. Zhang et al. showed their results of characterization of micron sized helical artificial bacterial flagella (ABFs) in water applying external rotating magnetic field [7]. They pointed out that size of the head and strength of applied magnetic field affect swimming velocity of ABFs [7]. The observations of swarm-like behavior of three independent ABFs controlled with rotating magnetic field with 2 mT field strength can also be found in this study [7].

Although there are different actuation methods proposed in the literature, like the mini DC brushless motor used in [8], the use of external magnetic fields has many advantages that circumvent the need for delivering power to the microrobot and ensuring autonomous untethered motion of the microrobot [9].

Work on the swimming of robots inside channels has significant relevance to in vivo applications. From medical perspective, the controllable motion of microrobots in arteries and capillaries becomes extremely important. For example, in an operation to open up a blood clot inside a hard to reach artery in a vital organ such as brain, a millimeter-sized robot must be delivered inside a nearby artery, navigated through the arterial network, asked to perform a task such as releasing of an anti-clotting agent, and navigated back for recovery. Honda et al. [10] demonstrated an externally actuated cm-long spiral microrobot with a SmCo magnet head propagating in a 15-mm diameter channel filled with silicone oil as a result of rotating magnetic field. Authors concluded that the motion of the robot is proportional the excitation frequency and can be predicted by the slender body theory of Sir Lighthill [11]. Similarly, Fountain et al. used a rotating permanent magnet (RPM) manipulator with a helical microrobot having a diameter of 1.625 mm and made experiments in lumen using gradients in nonuniform magnetic field [12]. It has been studied that RPM manipulator is viable for 1DOF propulsion and gradual steering maneuvers [12]. Martel et al. demonstrated that Magnetic Resonance Imaging (MRI) can be used as an actuation method for dragging magnetized particles [13] and Mathieu and Martel validated that in physiological circumstances with a magnetic sphere which has 1.5mm diameter in size by using magnetic field gradient [14]. They also used Maxwell coil pairs placed inside MRI to steer a magnetic microparticle in a microvascular channel [15].

Here we present swimming experiments of mm-sized microrobots in glycerol and water-filled mini channels and actuated by a rotating external magnetic field generated by two pairs of counter facing electromagnetic coils. Experiments are carried out for two swimming microrobots which consist of heads made of permanent magnets and rigid helical tails of different dimensions. The robots used in experiments have a radius of 180 and 230μm and length of 2.45 and 2.17mm and with these dimensions they simulate micro-fluidic regime since the same flow conditions as micro-scale rotation arise

when they are in glycerol-filled mini channels. Use of water as a working fluid in the experiments demonstrate the efficacy of microrobots in the low inertia regime where the Reynolds number based on the tails kinematic parameters is greater than 1. Moreover, experiments presented here are intended for detailed studies of the flow regimes outside the dominance of viscous forces especially by means of micro particle image velocimetry (PIV) [16, 17]. Lastly, the motion of the microrobot inside channels is ensured to follow a linear trajectory for comparisons with the theoretical results of Sir Lighthill [11].

II. Methodology

In what follows, the components of the experimental setup are discussed: fabrication and properties of the microrobots, properties of the electromagnetic coils which provide rotating magnetic fields, and the properties of the flow channels.

A. Fabrication of the Micro Swimmers

For medical applications, human circulatory system is the most important application area for untethered swimming of microrobots, since it is possible to reach every place of the body by vessels [4]. In order to use microrobots for performing in vivo missions such as targeted drug delivery, removing plaque, destroying blood clots, they should be navigated controllably in blood vessels, arteries and capillaries in which they can fit have diameters ranging from a few microns to centimetres [4]. Micro swimmers manufactured in our laboratory have diameters less than half a millimetre and lengths at most 3 mm. With these dimensions they seem ready to be used in small to medium arteries and other canals in the body with low flow rates [4].

Microrobots, which are used in this work, consist of a permanent magnetic head and a helical tail, which is made of metal wire. Magnetic head is the element that moves together with the rotating magnetic field. Helical tail is attached to the magnetic head with a strong adhesive and is in motion with respect to it.

1) Magnetic Head: In order to have high magnetization factor in small volumes, large pieces of neodymium-iron-boron (NdFeB) magnet powder are used. Nearly spherical lumps of magnets have dimensions that measure: $150\mu m \times 160\mu m \times 160\mu m$ (L2W3 in Fig. 1) and $160\mu m \times 170\mu m \times 170\mu m$ (L2W4 in Fig. 1) respectively. Each robot has a different size of magnetic particles because of the irregularity of the large pieces in the powder.

2) Helical Tail: The tail was made of the metal wires of diameter is 110 μm. Helices were produced by coiling the wires up on cylinders with different diameter. Wave lengths or wave numbers of helices were adjusted by simply deforming the helices. The dimensions of micro swimmers can be seen in Table 1.

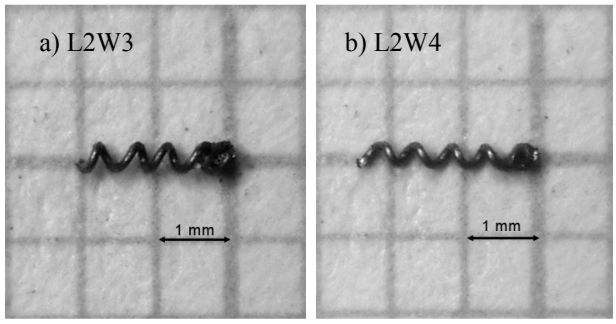

Fig. 1 Swimming microrobots made in the laboratory. a) L2W3 – shorter and thicker b) L2W4 – longer and thinner

TABLE I
Dimensions of Micro Swimmers

	Length [mm]	Number of waves	Length of tail [mm]	Diameter of head [mm]	Helice diameter [mm]
L2W3	2.17	3	1.71	0.46	0.41
L2W4	2.45	4	2.09	0.36	0.36

B. Experimental Setup

The use of alternating and rotating magnetic fields for propagation and steering of magnetic devices is a popular method of actuation for untethered robots [1, 2, 6, 10, 11, 18]. Usually, orthogonal electromagnetic coil pairs are used such as Helmholtz or Maxwell coils for achieving rotating magnetic fields. Pawashe et al. used six independent electromagnetic coil pairs and obtained a stick-slip motion of a microrobot [18], whereas Zhang et al. used three orthogonal coil pairs and attained uniform rotating magnetic field [2].

The forward and backward propagation of the micro swimmers are provided by applying rotating magnetic field. For manipulation of the robots four coils were placed by pairs being perpendicular to each other as seen in Figure 2. The magnetic head can rotate by means of the applied magnetic field only when magnetic torque on the head overcomes the viscous resistance of the fluid on the robot inside the channel.

The torque needed to rotate the micro swimmer is provided by the electromagnetic coils. If we represent magnetic dipole moment with $\boldsymbol{m}$ and magnetic induction with $\boldsymbol{B}$, the torque on a dipole in free space is [19]

$$\boldsymbol{\tau_M} = \boldsymbol{m} \times \boldsymbol{B} = \mu_0 \boldsymbol{m} \times \boldsymbol{H} \tag{1}$$

The magnetic particles having a magnetic moment vector $\boldsymbol{m}$ tend to align with the direction of the magnetic induction [19]. Magnetic dipole moment is a property of the material, and is given by the magnetization ($\boldsymbol{M}$) and the volume of the particle ($\mathcal{V}$).

$$\boldsymbol{m} = \boldsymbol{M} \times \mathcal{V} \tag{2}$$

Thus, one may recast (3) as follows:

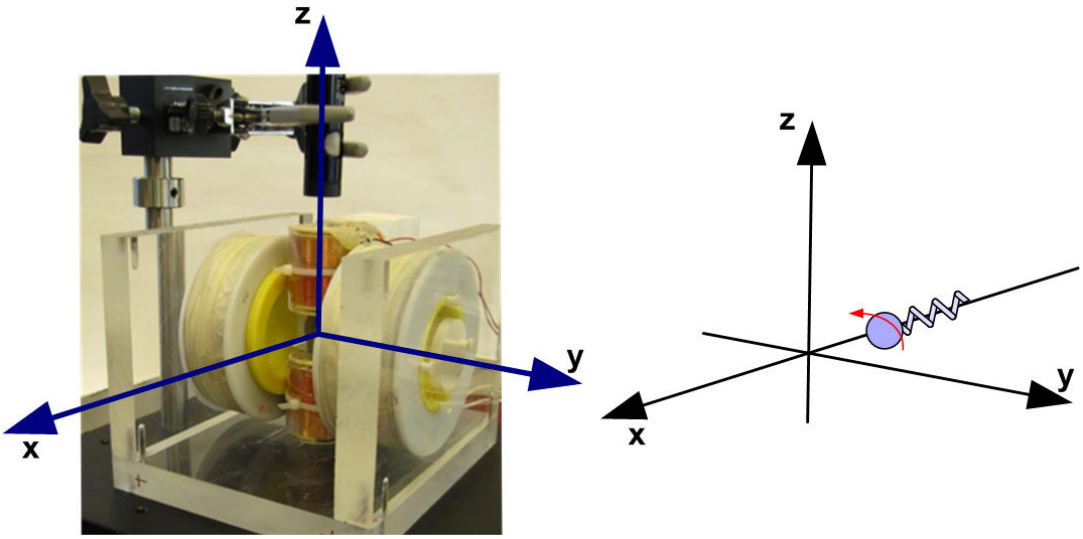

Fig. 2 Experimental setup consists of electromagnetic coil pairs and USB microscope camera can be seen on the left hand side. On the right side, schematic view of micro swimmer is represented.

$$\tau_M = \mu_0 \mathcal{V} M H \sin\theta \tag{3}$$

where H is magnetic field and θ is the angle between $\boldsymbol{B}$ and $\boldsymbol{m}$. Magnetic field along the axis of a circular coil depends on the current passing thru coil, I, radius of the coil, a, number of turns, N, and distance along the axis of the coil from the center, x, and is found by deriving Biot-Savart law as [19]

$$H = \frac{NIa^2}{2(a^2 + x^2)^{3/2}} \tag{4}$$

In order to rotate the magnetic particle attached to the helical tail, the magnetic torque supplied from the external field must be equal to the viscous torque on the whole swimmer:

$$C_B \begin{bmatrix} U \\ \Omega \end{bmatrix} + C_T \begin{bmatrix} U \\ \Omega \end{bmatrix} = \begin{bmatrix} F \\ \tau_M \end{bmatrix} \tag{5}$$

where, for a full six degree of freedom motion, C_B and C_T are the mobility matrices of the body and tail, U is the translational velocity, Ω is the rotational velocity, F is the external force applied (which is zero here), and τ_M is the magnetic torque. Since the body and tail are not separate links and attached to each other, U and Ω are same for body and tail.

$$\left(\begin{bmatrix} C_{B_\mathrm{N}} & 0 \\ 0 & C_{B_\mathrm{R}} \end{bmatrix} + \begin{bmatrix} C_{T_{\mathrm{N},1}} & C_{T_{\mathrm{N},2}} \\ C_{T_{\mathrm{R},1}} & C_{T_{\mathrm{R},2}} \end{bmatrix} \right) \begin{bmatrix} U \\ \Omega \end{bmatrix} = \begin{bmatrix} F \\ \tau_M \end{bmatrix} \tag{6}$$

Components of mobility matrices of body and tail are different from each other. Derivation of the mobility matrix components can be found in [20]. Normal and tangential force coefficients for tail can be calculated theoretically with the derivations Sir Lighthill stated in 1976 [11]. For a spherical body, C_{B_N} and C_{B_R} are written as

$$C_{B_\mathrm{N}} = -6\pi\eta r^2 \tag{7}$$

$$C_{B_\mathrm{R}} = -8\pi\eta r^3 \tag{8}$$

where η is the viscosity of the fluid and r is the radius of the spherical head [20].

The electromagnetic coils in our setup are not identical (see Table 2). In order to obtain a uniform magnetic field everywhere in the working space, ideally, the distance between the coils must be equal to the average radius of the coils. The magnetic field is uniform enough for the workspace, which is used in the experiments and consists of a glass pipette of 1-mm-inner diameter; observations are made for about 10-mm swimming range of the robot.

Electromagnetic coils are mounted as shown in Figure 2. Alternating current is applied to obtain a rotating magnetic field. The current is transmitted to the coils from the power generators via Maxon ADS_E 50/10 motor drives that are connected to DS1103PPC controller board.

The magnitude of current and frequency of the sinusoidal currents are adjusted by the ControlDesk software. Maxon motor drives are operated with dSPACE and the signal is converted from digital to analog. Each coil is connected to one Maxon motor drive. Alternating current is applied to coil pairs with a phase shift to obtain the rotating magnetic field. The current applied to the small and big coils are defined as $I_{SC} = I_{0,SC}\sin(2\pi f t)$ and $I_{BC} = I_{0,BC}\cos(2\pi f t)$ respectively.

Propagation of micro swimmers is observed with TIMM-400 S/W v. 0.1-100 Microscope having a resolution of 720×576 pixels in which a USB digital camera that can record maximum 30 frames per second is mounted.

The micro swimmers are placed in glass pipettes filled with glycerol and water. The pipettes are placed on the x axis

which is shown schematically in Figure 2. Experiments are conducted for five different magnetic field strengths in glycerol with micro swimmers L2W3 and L2W4. The L2W4 is also used in water under three different magnetic field strengths.

TABLE II
DIMENSIONS OF COILS

Coils	y axis	z axis
Measured resistance [Ω]	14	7.5
Wire diameter [mm]	0.45	0.8
Number of turns	1400*	750
Coil diameter [mm]	30	90
Distance between coils [mm]	20	60

*Since the data sheet is not available, this information was obtained by calculations and may not be precise.

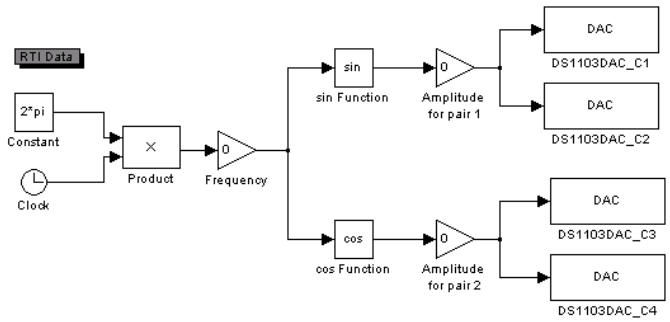

Fig. 3 Simulink blocks for implementation in dSPACE

III. RESULTS

A. Experiments in Glycerol

The micro swimmer L2W3 and L2W4 are placed in a glass pipette having an inner diameter of 1 mm, and pipette is filled with glycerol having a dynamic viscosity of 0.1 Pa·s . Reynolds number is calculated for both head and tail assuming the head is perfect sphere at 10 Hz. Density of the fluid, linear velocity of micro swimmer, radius of head, rotation frequency, diameter of the tail and amplitude of helical tail wave are represented with ρ, V, r, f, d and A respectively.

$$Re_{\text{head\_L2W3}} = \frac{\rho V r}{\eta} = 2.4 \times 10^{-3} \quad (9)$$

$$Re_{\text{tail\_L2W3}} = \frac{2\pi f A d \rho}{\eta} = 12.8 \times 10^{-3} \quad (10)$$

Although the Reynolds numbers are greater than the Reynolds number of bacteria in water, they are still much smaller than 0.1. Thus, inertial effects are negligible with respect to viscous forces.

In Figure 4 and 5, linear velocities of micro swimmer L2W3 and L2W4 in glycerol are represented with respect to magnetic field strength and rotating frequency. Five different magnetic field strengths changing from 6.85 mT to 7.60 mT are used in the experiments; rotating frequency is varied from 5 Hz to50 Hz.

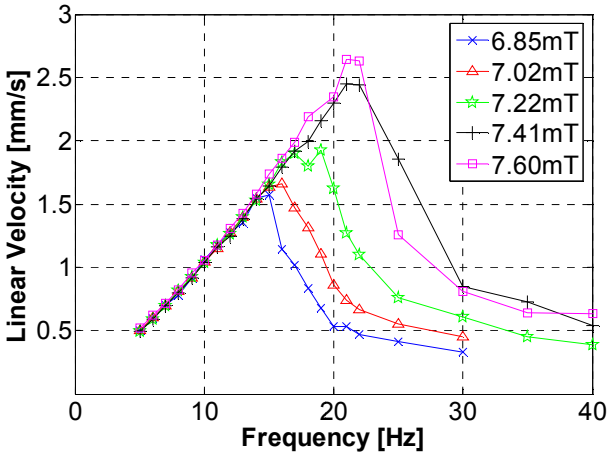

Fig. 4 Dependence of linear velocity of micro swimmer L2W3 on magnetic field strength and rotation frequency

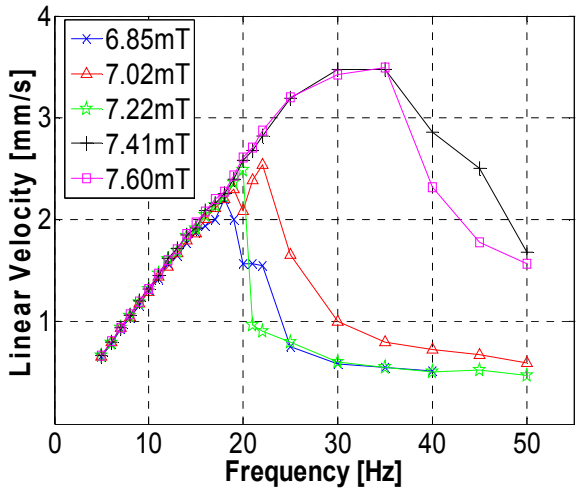

Fig. 5 Dependence of linear velocity of micro swimmer L2W4 on magnetic field strength and rotation frequency

The linear velocity is obtained by dividing the distance to the time that micro swimmer takes to travel. For both robots the same behavior is observed. The linear increase in velocity continues up to a maximum point, where the swimmer starts to slow down due to insufficient magnetic torque, which no longer can make the swimmer rotate with the frequency of rotating magnetic field. This behavior can also be seen both in micro [7] and macro scales [10]. Maximum linear velocity is obtained as 2.65 mm/s for L2W3 and 3.5 mm/s for L2W4, under the effect of 7.60 mT. Because of the linear relationship between velocity and frequency, it is clear that applying stronger magnetic field at higher frequencies will result with increment in linear velocity. The frequency value at which the micro swimmers reach their maximum linear velocity is known as step-out frequency.

$$Re_{\text{head\_L2W4}} = \frac{\rho V L}{\eta} = 2.4 \times 10^{-3} \quad (11)$$

$$Re_{\text{tail\_L2W4}} = \frac{2\pi f A d \rho}{\eta} = 18.1 \times 10^{-3} \quad (12)$$

In Figure 6 the comparison in velocities of L2W3 and L2W4 can be seen. The data represented are obtained under 7.02 mT magnetic field strength. As expected, L2W4 travels faster than L2W3, since the former has a longer tail with more waves, which increases the propulsive force, and a smaller head that decreases the drag.

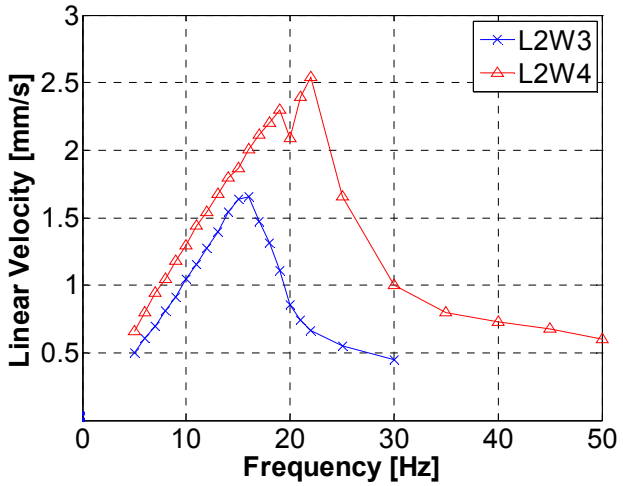

Fig. 6 Comparison of L2W3 and L2W4 in terms of linear velocity. Applied magnetic field strength is 7.02mT

Resistive force theory [21] is applied to the swimmers in order to compare the experimental results. In Figure 7, the comparison of experimental results with normal and tuned RFT for L2W4 at 7.60 mT is represented. The theoretical normal and tangential drag coefficients for tail and body are calculated from [11, 20] and then tuned to include the wall effects.

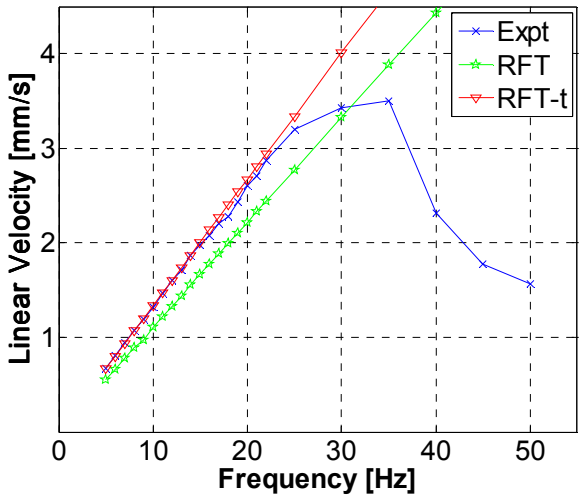

Fig. 7 Comparison of experimental data collected at 7.60mT with the RFT model. The data match perfectly with each other.

B. Experiments in Water

The micro swimmer L2W4 was placed in a glass pipette having an inner diameter of 1 mm, and pipette is filled with water which has a dynamic viscosity of 0.001 Pa·s. Previous assumptions about Reynolds number and inertial and viscous effects are no longer applicable to the experiments in water. At 30 Hz, the Reynolds numbers of the head's and tail's motion are as follows:

$$Re_{\text{head\_L2W4}} = \frac{\rho V L}{\mu} = 0.55 \quad (13)$$

$$Re_{\text{tail\_L2W4}} = \frac{2\pi f A d \rho}{\mu} = 5.43 \quad (14)$$

In Figure 8, the results of the experiments in water are presented. Three different magnetic field strength are applied; 5.70 mT, 6.00 mT, 6.45 mT. Up to 50 Hz, the effect of magnetic field strength does not make a difference in linear velocities. At 20 Hz, micro swimmer is slower in water than it is in glycerol, so we can conclude that inertial effects are not negligible and deteriorates the propulsion of the helical tail. Increasing frequency more than 50 Hz results in an unpredictable velocity behavior, due to more pronounced inertial effects, as $Re_{\text{tail\_L2W4}}$ is on the order of 10.

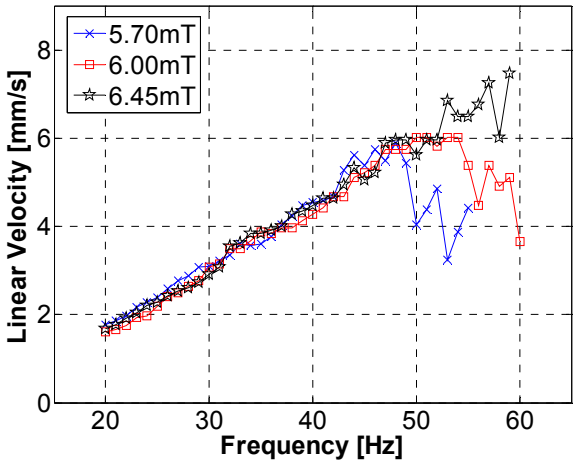

Fig. 8 Dependence of linear velocity of micro swimmer L2W4 on magnetic field strength and rotation frequency in water. The behavior after step-out frequency is a reason to be suspicious about inertial effects

IV. Conclusions

Experiments with two micro swimming robots that have scales (0.36 and 0.41 mm in diameter and 2.17 and 2.45 mm in length), which are compatible with medical use in the human circulatory system are presented here. The micro swimmers used in experiments are made of permanent NdFeB magnet heads and helical metal-wire tails. Microrobots are actuated by external rotating magnetic fields and the swimming behaviors are observed in glycerol and water-filled glass channels. To attain rotational magnetic field, out of

phase alternating currents are applied to two orthogonal electromagnetic coil pairs.

The range of the Reynolds number for experiments with glycerol shows that inertial effects are negligible similar to typical flow conditions of microscopic organisms. Thus, the linear relationship between rotating frequency and the velocity of the micro swimmer is observed for frequencies less than step-out frequency. The range of the Reynolds number for experiments in water is well above unity and up to 10 for the highest velocity observed in the experiments. Thus, clearly inertial effects are significant for mm-long microrobots swimming in water and similar fluids. Although a linear relation between frequencies and velocities are observed for up to 40 Hz, the microrobot travels slower in water between 20 Hz and 40 Hz than in glycerol owing to the significance of the inertial effects.

Experiments conducted in glycerol indicated that the size of head and tail is important. The comparison of the results measured from two different micro swimmers shows that the one with smaller head and longer tail travels faster. There are two outcomes from this observation: the first is the drag force of the head must be minimal to increase the speed of the robot as also observed elsewhere [7]. The second is that the longer tail with more helical turns (waves) improves the propulsion force of the tail.

Experimental data are confirmed with the resistive force theory for low Reynolds number motion of the swimmer. The behavior of microrobots swimming in glycerol is compared to results obtained from resistive force theory where the change in linear velocity with respect to frequency shows a linear relationship and agrees well with experimental data after tuning up to step-out frequency. Future work will include the comparison of linear velocities obtained from experiments and RFT with respect to wave number and wave amplitude of tail.

REFERENCES

[1] R. Dreyfus, J. Baudry, M. L. Roper, M. Fermigier, H.A.Stone, and J. Bibette, "Microscopic artificial swimmers," *Nature,* vol. 437, pp. 862-865, Oct. 2005.

[2] Zhang, J. J. Abbott, L. Dong, B. E. Kratochvil, D. Bell, and B. J. Nelson, "Artificial bacterial flagella: fabrication and magnetic control," *Applied Physics Letters*, vol. 94, pp. 064107-1-3, February, 2009.

[3] A. Ghosh and P. Fischer, "Controlled propulsion of artificial magnetic nanostructured propellers," *Nanoletters,* vol. 9, no. 6, pp. 2243-2245, March, 2009.

[4] B. J. Nelson, I. K. Kaliakatsos, and J. J. Abbott, "Microrobots for minimally invasive medicine," *Annu. Rev. Biomed. Eng.,* vol. 12, pp. 55-85, April, 2010.

[5] J. Edd, S. Payen, M. Sitti, M. L. Stoller, and B. Rubinsky, "Biomimetic propulsion mechanism for a simming surgical micro-robot," *Proc. IEEE/RSJ Int. Conf. on Intelligent Robots and Systems*, pp.2583-88, Las Vegas, USA, October 2003.

[6] S. Sudo, S. Segawa, and T. Honda, "Magnetic swimming mechanism in a viscous liquid," *Journal of Intelligent Material Systems and Structures,* vol. 17, pp. 729-736, August-September 2006.

[7] L. Zhang, J. J. Abbott, L. Dong, K. E. Peyer, B. E. Kratochvil, H. Zhang, C. Bergeles, and B. J. Nelson, "Characterizing the swimming properties of artificial bacterial flagella," *Nano Letters,* vol. 9, no. 10, pp. 3663-3667, August 15, 2010.

[8] B. Behkam and M. Sitti, "Design methodology for biomimetic propulsion of miniature swimming robots," *ASME Journal of Dynamic Systems, Measurement, and Control*, vol. 128, no.1, pp. 36-43, March 2006.

[9] J. J. Abbott, K. E. Peyer, M.C. Lagomarsino, L. Zhang, L. Dong, I. K Kaliakatsos, and B. J. Nelson, "How should microrobots swim?," *The International Journal of Robotics Research,* vol. 28, pp. 1434-1447, November-December 2009.

[10] T. Honda, K. I. Arai, and K. Ishiyama, "Micro swimming mechanisms propelled by external magnetic fields," *IEEE Transactions on Magnetics,* vol. 32, pp. 5085-5087, Sept. 1996.

[11] Sir J. Lighthill, "Flagellar hydrodynamics: the John von Neumann lecture," *SIAM Review*, vol. 18, no. 2, pp. 161-230, April, 1976.

[12] T. W.R. Fountain, P. V. Kailat, and J. J. Abbott, "Wireless control of magnetic helical microrobots using a rotating permanent magnet manipulator," IEEE *International Conference on Robotics and Automation,* May 2010.

[13] S. Martel, J-B. Mathieu, O. Felfoul, H. Macicior, G. Beaudoin, G. Soulez, and L'H. Yahia, "Adapting MRI systems to propel and guide microdevices in human blood circulatory system," *Engineering in Medicine and Biology Society, 2004. IEMBS '04. 26th Annual International Conference of the IEEE* , vol.1, pp.1044-1047, Sept. 2004.

[14] J-B. Mathieu and S. Martel, "In vivo validation of a propulsion method for untethered medical microrobots using a clinical magnetic resonance imaging system," *Proc. in IEEE/RSJ International Conference on Intelligent Robots and Systems,* Oct.-Nov. 2007.

[15] J-B. Mathieu and S. Martel, "Magnetic microparticle steering within the constraints of an MRI system: proof of concept of a novel targeting approach," *Biomed Microdevices*, vol.9, pp. 801-808, 2007.

[16] C. D. Meinhart, S.T. Wereley, and J.G. Santiago, "PIV measurements of a microchannel flow," *Experiments in Fluids,* vol. 24, pp. 414-419, 1999.

[17] H. Nasibov, A., Kholmatov, B. Akselli, A. Nasibov and S. Baytaroglu, "Performance analysis of the CCD pixel binning option in particle-image velocimetry measurements," *IEEE/ASME Transactions on Mechatronics,* vol. 15, pp. 527-540, August 2010.

[18] C. Pawashe, S. Floyd, and M. Sitti, "Modeling and experimental characterization of an untethered magnetic micro-robot," *The International Journal of Robotics Research*, vol. 28, no. 8, pp. 1077-1094, August, 2009

[19] D. Jiles, *Introduction to Magnetism and Magnetic Materials*, 2nd ed., Ed. London, UK: Chapman & Hall, 1998.

[20] A. F. Tabak and S. Yesilyurt, "Validated reduced order models for simulating trajectories of bio-inspired artificial micro-swimmers," *Proc. in ASME FEDSM-ICNMM2010,* no.30857, August 2010.

[21] J. Gray and G. J. Hancock, "The propulsion of sea-urchin spermatozoa," *J. Exp. Biol.*, vol. 32, pp. 802-814, 1955.